Nuclear Instruments and Methods in Physics Research A 354 (1995) 338–351

ELSEVIER

NUCLEAR INSTRUMENTS & METHODS IN PHYSICS RESEARCH Section A

Performance of a prototype tracking detector for double beta decay measurements

NEMO Collaboration

R. Arnold [b], A. Barabash [d], D. Blum [f], V. Brudanin [e], J.E. Campagne [f], F. Danevich [c], D. Dassié [a], V. Egorov [e], R. Eschbach [a], J.L. Guyonnet [b], F. Hubert [a], Ph. Hubert [a], M.C. Isaac [a], C. Izac [a,*], S. Jullian [f], O. Kochetov [e], V.N. Kornoukov [d], V. Kouts [c], V. Kovalenko [e], D. Lalanne [f], T. Lamhamdi [b], F. Laplanche [f], F. Leccia [a], Yu. Lepikhin [d], I. Linck [b], C. Longuemare [g], F. Mauger [g], P. Mennrath [a], F. Natchez [f], H.W. Hicholson [h], A. Nozdrin [e], G. Pichenot [f], F. Piquemal [b], F. Scheibling [b], C.S. Sutton [h], G. Szklarz [f], V.I. Tretyak [c], V. Umatov [d], I. Vanushin [d], Yu. Vassilyev [c], A. Vareille [a], Ts. Vylov [e], Sh. Zaparov [e], Yu. Zdesenko [c]

[a] *CENBG, IN2P3-CNRS et Université de Bordeaux I, 33175 Gradignan Cedex, France*
[b] *CRN, IN2P3-CNRS et Université Louis Pasteur, 67037 Strasbourg, France*
[c] *INR of the Ukrainian Academy of Sciences, Kiev, Ukraine*
[d] *ITEP, Moscow, Russian Federation*
[e] *JINR, Dubna, Russian Federation*
[f] *LAL, IN2P3-CNRS et Université de Paris Sud, 91405 Orsay, France*
[g] *LPC, IN2P3-CNRS et Université de Caen, 14032 Caen, France*
[h] *Mount Holyoke College, South Hadley, MA 01075, USA*

Received 22 July 1994

Abstract

To investigate double beta decay processes, the NEMO collaboration began a long-range research and development program in 1988. The NEMO 2 detector, which is now running in the Fréjus underground laboratory (L.S.M. Laboratoire Souterrain de Modane), is the second prototype. It consists of a 1 m^2 source foil sandwiched between Geiger cell drift chambers for electron tracking and two plastic scintillator walls for energy and time-of-flight measurements. The technical description of the detector is followed by the study of the various sources of background.

1. Introduction

The double beta decay process is a de-excitation of a nucleus which releases simultaneously two electrons either with ($\beta\beta 2\nu$) or without ($\beta\beta 0\nu$) neutrinos in the final state. The ($\beta\beta 0\nu$) decay mode, which has not yet been observed, constitutes a very sensitive test of the existence of a massive Majorana neutrino and right-handed weak currents [1]. Thus the observation of this process would indicate physics beyond the standard model. The ($\beta\beta 2\nu$) decay, as a second order electroweak transition, is completely described by the standard model and has already been experimentally observed. Research on this process is a useful test of the theoretical models involved in the calculation of the nuclear matrix elements. Another decay mode may also occur, the ($\beta\beta 0\nu,\chi$) where a hypothetical light neutral boson χ, the Majoron, is emitted. Decay modes which are less favorable by phase space considerations are $\beta^+\beta^+$, β^+ with electron capture, and two electron capture decays. Experimentally the $\beta\beta$ decay modes can only be distinguished by their different electron energy spectra. The theoretical sum energy spectra of the electrons emitted during these decay modes are represented in Fig. 1.

The NEMO experiment is one of a number of experiments that study $\beta\beta$ decay processes by the direct detec-

* Corresponding author. e-mail izac@frcpn11.in2p3.fr.

SSDI 0168-9002(94)01025-0

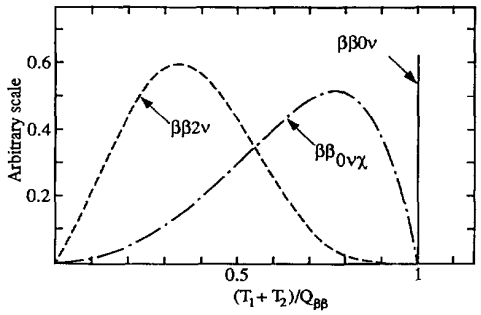

Fig. 1. Illustration of the summed electron energy spectra for the $(\beta\beta 2\nu)$, $(\beta\beta 0\nu)$ and $(\beta\beta 0\nu, \chi)$ decays.

tion of the emitted electrons [2–4]. Currently the NEMO collaboration is building a detector to utilize 10 kg of an enriched molybdenum source in order to reach a sensitivity limit of 10^{25} years for the half-life of the $(\beta\beta 0\nu)$ mode. Such a sensitivity would be an order of magnitude gain on the current experimental limit on the neutrino's effective mass ($\langle m_\nu \rangle \leq 1$–$2$ eV, [2]).

The first prototype, NEMO 1, was built three years ago. This detector was composed of 64 multiwire drift tubes operating in the Geiger mode. The tracking volume, filled with helium gas at atmospheric pressure, was sandwiched between two horizontal plastic scintillator planes. The energy information and the trigger were provided by photomultiplier tubes (PMTs) and associated scintillators. Helium was chosen as the tracking gas because it is almost transparent to low energy electrons, and thus minimizes multiple scattering effects. This prototype ran with stability and reliability for 18 months in the Fréjus underground laboratory, and demonstrated that electron tracking is possible for electrons with energy as low as 100 keV. The events contributed by cosmic rays, neutrons and natural radioactivity in the recorded background spectra were identified [5].

The NEMO 2 detector, a second prototype ten times larger than NEMO 1, was constructed using a similar detection system. This detector houses a thin central source. It records the tracks of electrons emitted from the source while attenuating the background rate by time-of-flight (t-o-f) measurements. The experiment is located in the Fréjus underground laboratory. Although designed for background studies, the NEMO 2 detector demonstrated sufficient sensitivity to measure $(\beta\beta 2\nu)$ in the range of a few times 10^{19} years.

The NEMO 2 detector and its operation are described in the first part of this article. Then the influence of the various background sources such as natural radioactivity, radon, cosmic rays and neutrons is discussed. A brief description of the detector has already been presented [6], while the preliminary results of a search for ββ decay of ^{100}Mo are given elsewhere [7,8].

2. Description of the NEMO 2 detector

2.1. General design

NEMO 2 is made of a 1 m^2 source foil, a 1 m^3 volume filled with drift chambers composed of Geiger cells and two plastic scintillator arrays. The experimental configuration, with the shield removed, is shown in Fig. 2. The tracking volume is filled with helium gas at atmospheric pressure. Thin source foils can be mounted on a 1 m^2 central frame sandwiched between cell planes. The two external arrays of plastic scintillator measure energies and t-o-f of the detected particles. Each scintillator array is 50 cm away from the central source which enables the use of t-o-f as a rejection criterion for incoming electrons in a compact detector. The different components of the shielding, their thickness and relative position, were studied in the NEMO 1 prototype and have been scaled accordingly in NEMO 2. In order to optimize both the efficiency and cost of the shielding, an internal 5 cm layer of lead was surrounded by a 20 cm layer of iron. The 1 MeV photons generated by the weak ^{60}Co activity contained in the iron (≈ 0.02 Bq/kg, as measured by γ-ray spectroscopy), are strongly attenuated by the internal lead layer and the thick copper plate framework of the drift chamber and scintillator arrays. Circulation of air within the shield moderates the build-up of helium which would damage the PMTs, while cooling the voltage dividers which collectively release approximately 300 W.

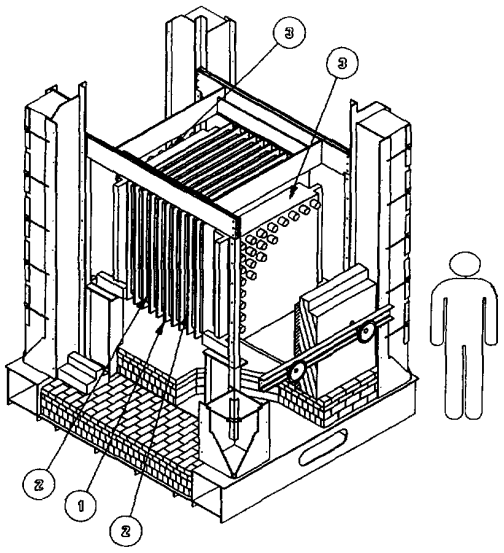

Fig. 2. Diagram of the experimental configuration. 1 – Central frame supporting the source. 2 – Copper frames which support the Geiger cells. 3 – 8×8 arrays of scintillator counters.

2.2. The tracking device

The whole tracking device is enclosed by two 1 m^2 aluminized mylar sheets 36 μm (700 Å of Al) thick which ensure the confinement of helium while imposing only small energy losses to electrons. On each side of the central foil are 5 copper frames composed of two parallel planes of 32 horizontal wire cells and 32 vertical wire cells. This alternation of horizontal and vertical cells provides accurate tracking. It also ensures the same tracking precision on the top and side projection views of the drift chamber which are used in track reconstruction. The gap between two planes of cells within a frame is 32 mm.

A Geiger cell is sketched in Fig. 3. Each octagonal cell is 32 mm in diameter and 1 m in length with a central anode wire surrounded by 8 grounded wires. At the ends of a cell are cathode pickup electrodes made of a copper ring. High voltage (1800 V) is applied to the anode wire. When a charged particle crosses a cell, the ionization of the helium creates on the average six primary electrons per centimeter which drift toward the anode wire at a speed of 1 cm/μs. The resulting plasma on the central wire then propagates toward the ends of the cell at a speed of 6 cm/μs. The average trigger rate of each cell during operation is 0.05 Hz. The efficiency of each cell is greater than 99%.

Conventional electronics (CAMAC and NIM) are used in the readout electronics of the tracking device. The drift time of the electrons gives the transverse position relative to the central wire by the use of a TDC (80 MHz scaler) which records the time difference between the anode signal and the delayed signal of the plastic scintillators. The cathode pulses provide the propagation time of the plasma with two TDC units that measure the time differences between the anode signal and the two cathode pulses in order to find the longitudinal position which is deduced from the difference in the propagation times. A sample of the two propagation times for the Geiger cells are represented in Fig. 4. This figure shows that the sum of the measured times is constant for any recorded position and therefore demonstrates the homogeneity of the wire cells.

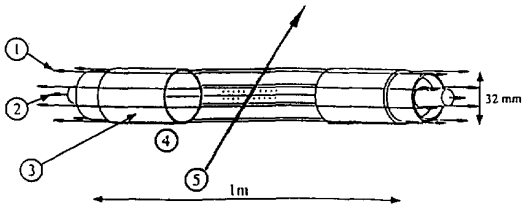

Fig. 3. Elementary Geiger cell. 1 – Eight grounded wires, diameter 100 μm, length = 1 m. 2 – Central anode wire, diameter 100 μm, length = 1 m, H.V. = +1800 V. 3 – Cathode ring (Ø = 29 mm). 4 – Helium gas (atmospheric pressure) + 4% ethyl alcohol. 5 – Through going particle and induced charges.

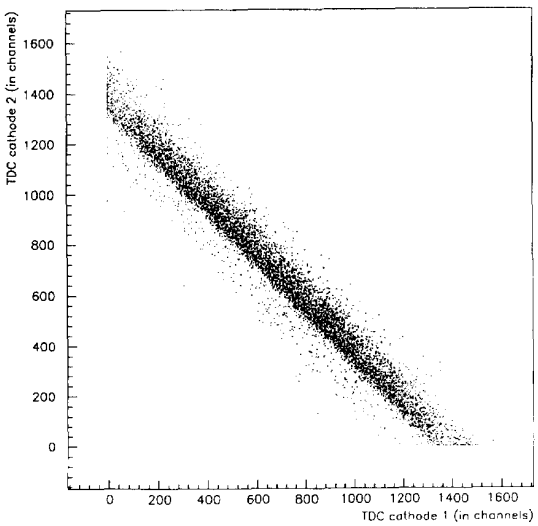

Fig. 4. Distribution of the propagation times of the plasma along the wire.

The three-dimensional track of a charged particle is reconstructed from these longitudinal and transverse coordinates as extracted from the cells which have fired. The detector is also equipped with "slow TDCs" on the anodes which can record delayed events from 1 μs to 1 ms after trigger.

The gas in the detector is helium with 4% ethyl alcohol operating at 1 mbar above atmospheric pressure. The alcohol has a quenching effect which ensures stable functioning of the Geiger cells. It absorbs the secondary UV light emitted by the plasma of a Geiger cell thus minimizing possible triggers of neighboring cells. Two security systems are incorporated to cope with large pressure variations inside the laboratory. The hybrid helium system has internal gas circulation and open flow.

The average density of gas in the sensitive volume is 0.2 mg/cm^3 which yields an energy loss of 14 keV for a 1 MeV electron crossing 50 cm of the gas detector. This enables the tracking of electrons with energy as low as 100 keV. The helium is stored in bottles at a maximum pressure of 200 bar and is sent into the system via a regulator/pressure gauge at 30 mbar. The flow rate is 15 1/h. Electron tracking requires a high purity gas so the purity of the entering helium is monitored for oxygen contamination ($\lesssim$ 3 ppm) before being bubbled through a container of alcohol that is kept at a constant temperature (11°C). The required concentration of alcohol is reached by saturating the helium with alcohol.

2.3. The plastic array detector

There are 64 identical scintillators in each of the two arrays with an 8 by 8 format. The front face of the

Table 1
Trigger types

Trigger conditions	Event type recorded	Counting rate (Hz)
≥ 1 counter on a wall	PMT singles	500
≥ 2 counters	PMT coincidences	2
≥ (1 counter + 1 track)	(e), (e, e), (e, γ), (e, γ, γ), (e, e, γ)	1.6
(1 counter + 1 track)	(e)	1.35
≥ (2 counters + 1 track)	(e, e), (e, γ), (e, γ, γ), (e, e, γ)	0.25

scintillators are 12×12 cm^2 and they are 2 cm thick. The plastic scintillator thickness was chosen to stop electrons with energies up to 4 MeV. Each detector module is composed of the above-mentioned scintillator block (NE110) with a 2.5 mm thick CsI(Na) layer on the back face of the blocks. The CsI layer was employed to tag X-rays from internal conversion electrons arising from the radioactive impurities of the central foil. The scintillator blocks were then attached to 90 mm thick light guides coupled to the PMT by a flexible silicon disk.

The NE110 scintillators are well-suited for the experiment because of their fast signal which enables good timing resolution. In addition, back scattering of the electrons is limited in the plastic scintillator because its components have low atomic numbers. The faces of the scintillators have been machined with a diamond tool. A teflon ribbon (2.6 mg/cm^2) is used to wrap the light-sensitive elements. It was chosen for its low level of radioactivity and its excellent diffuse reflection properties. Two layers of teflon were stretched over the front face of the scintillator and four layers on the others. In addition the front face was covered by a 2.5 μm film of aluminized (700 Å) mylar. Finally, the detector module was made light tight with a 2.0 mg/cm^2 black polycarbonate foil.

The mechanical support of the detector modules is provided by a copper frame (5 cm thick) and the PMT bases are surrounded by 10 cm lead shields. Both the copper frame and lead shield are designed to reduce the γ-ray flux generated by the PMTs. Finally an optical fiber, used for energy and timing calibrations, was inserted into a thin brass tube and affixed to the photocathode. A detector module is shown in Fig. 5.

2.4. Trigger and data acquisition

In the normal acquisition mode a two stage trigger must be satisfied to initiate the readout system. The first trigger level is generated by the scintillator chain. The second trigger level, which occurs 2.5 μs later, is derived from the Geiger cells. The resulting common trigger, which enables the readout detection of electron–electron and electron–gamma events thus requires at least two scintillators to fire in a time interval of 50 ns, and the activation of at least four Geiger cells belonging to different frames on one side of the central source (1 track). The different possible triggers and the corresponding event types and counting rates are reported in Table 1. The dead time in the usual trigger conditions is 3%. The dead time is dominated by the 1 ms window given to the "low TDCs" devoted to the measurement of delayed background events.

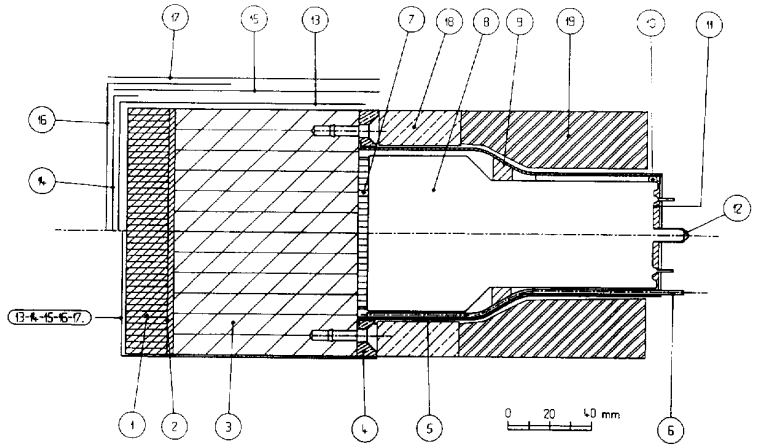

Fig. 5. Diagram of a detector module. 1 – NE110 scintillator. 2 – CsI(Na) scintillator. 3 – Light guide. 4 – Copper bedplate (1 cm). 5 – Copper shielding. 6 – Brass pipe for optical fiber. 7 – Silicone optical joint. 8 – PMT (XP2312). 9 – Soft plastic ring for positioning. 10–11 – 12 Silicone support inserts. 13 – Teflon reflector. 14 – 2.5 μm aluminized mylar reflector (700 Å Al). 15–16 – Polycarbonate for a light tight enclosure (20 μm). 17 – Copper sheet for mechanical protection (34 μm). 18 – Copper frame (5 cm). 19 – PMT's lead shield (10 cm).

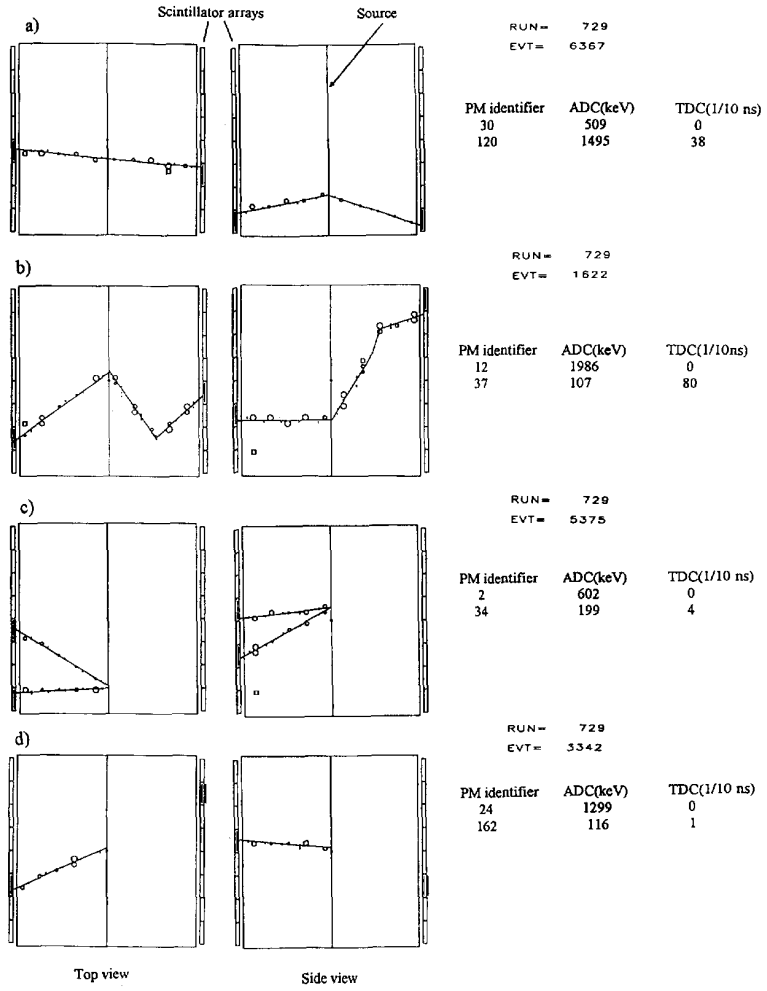

Fig. 6. Projected views of raw data events recorded in NEMO 2. The circles and bars represent the transverse and longitudinal position. The radius of the circles represent the detected position with respect to the central anode wire. a) An electron crossing the detector from left to right. b) An electron crossing the detector scattering once in the helium. c) Two electrons emitted from the central foil. d) An electron and a photon emitted from the central foil.

Data stored in CAMAC modules are read out with a 68020 micro-processor, under the OS9 operating system, through a VME–CAMAC interface. The acquisition program in response to a trigger reads out the data and stores it in a direct access "data-module". When a data-module is full (approximately 0.5 Mbytes) the data is immediately transferred through an Ethernet network to a micro-Vax 3300 located at the experimental site. In the transfer process the data is decoded and re-organized into ZEBRA [1] files. The possibility of easily adding information, such as calibrated energies and times, to the initial experimental data was a strong argument in the choice of the ZEBRA standard.

Since 16 Mbytes of experimental data are collected daily it is necessary to implement a filter. Among the recorded events, 95% are Compton electrons originating in scintillators that cross the tracking volume. These events are easily rejected by t-o-f selection. Here the ADC and TDC information is used in the track reconstruction procedure to calculate the t-o-f. The events are then filtered with a 3 ns cut and the rate of the raw data is reduced by a factor of seven. This reduction factor can be increased to 30 with more restrictive timing conditions and by taking into account the topology of the event and the deposited energies.

The experiment is run and controlled remotely by the

[1] ZEBRA user guide, Prog. Lib. CERN, Q100.

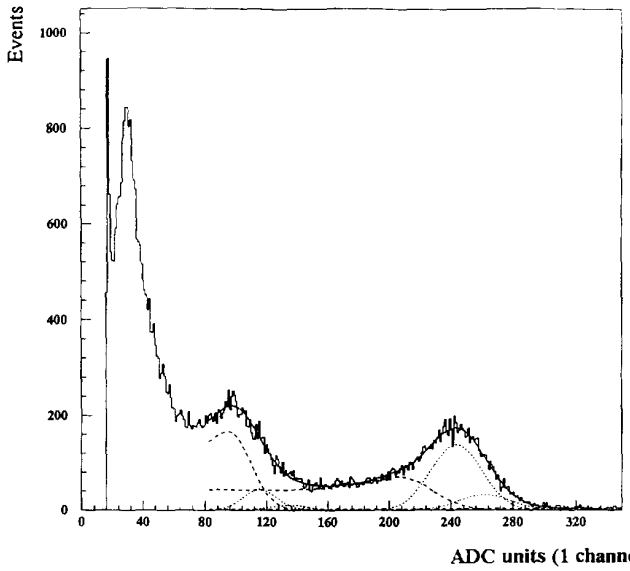

Fig. 7. Energy spectrum obtained with a ^{207}Bi source. The solid line is the result of a fit. Also shown are the various computed contributions to the spectrum from electrons (dotted lines), and photons (dashed lines).

different laboratories of the collaboration through a computer network which also provides data transfer for the data analysis.

3. Detector performances

3.1. Tracking device

In order to determine the transverse position, an empirical formula was developed which relates the drift time of the ionization electrons to the distance of the charged particle trajectory from the anode wire. This formula was established with the previous prototype NEMO 1 [5] and specific numbers computed with cosmic-ray muon data recorded by NEMO 2 before installation in the underground laboratory. The software track reconstruction measured the average transverse position with an accuracy of $\sigma = 500$ μm. This accuracy decreases slightly for tracks close to the central wire or at the edge of the cell. This accuracy can be considered as the optimum accuracy of a cell because muons suffer negligible multiple scattering. Concerning the longitudinal coordinate, calculated from the two cathode TDC values, the standard deviation is $\sigma = 4.7$ mm. This value is larger than the transverse one, but does not significantly affect the precision of the tracking because of the alternating horizontal and vertical cell planes.

A pattern recognition program gives a geometrical interpretation of the events. The resulting information is coded and added to the ZEBRA banks. In a first version the electron trajectories are assumed to be linear. The longitudinal and transverse coordinates relative to the cells are fitted to a straight line. The reconstruction program provides the direction cosines of the tracks and the (x, y) coordinates of the intersection of the tracks with the scintillator planes and the central source foil. This program is also able to tag the possible scatterings in the Geiger chamber or the back-scattering on the front faces of the scintillators. This program has also been used to filter the data.

A second reconstruction program was also implemented. This program takes into account all of the information given by the Geiger cells and the effects of multiple scattering. It is based on an iterative method of track recognition [9], which uses the Kalman algorithm. This reconstruction program gives the vertex position on the central foil with an accuracy of $\sigma_{(x, y)} = 0.5$ cm and a reconstruction efficiency close to 100%.

A software program running under the G.K.S. [2] standard provides a display of the reconstructed tracks. Different types of events that have been processed with the reconstruction program are shown in Fig. 6.

3.2. The energy and time-of-flight measurements

The absolute energy calibration of each scintillator is obtained by measurements using 3700 Bq electron and gamma sources (^{207}Bi, ^{137}Cs, and ^{88}Y). The source is positioned 4 cm away from the front face of each scintilla-

[2] G.K.S.: ANSI X3.124-1985 and ISO 7942-1985 "Graphical Kernel System".

tor by means of a moveable source carrier. The γ-ray Compton edges and the electron conversion lines (Fig. 7) are fitted with a minimum chi-squared method which provides the linear calibration parameters. The computed slopes and intercepts obtained from the three different sources for the same scintillator agree to within 1%, which gives good confidence in the calibration procedure. The response function of the scintillators to incident electrons is well-represented by a gaussian whose full width at half maximum (FWHM) (averaged over the 128 counters) is described by the empirical formula,

$$\mathrm{FWHM} = (28E + 2300)^{1/2}. \quad (1)$$

Here E is the energy measured in the scintillator, both E and FWHM are expressed in keV.

This corresponds to an energy resolution of 17.4% at 1 MeV. The first contribution, $(E)^{1/2}$, comes from statistical fluctuations while the second and constant term is related to the electronic noise. Note that NEMO 2 can be self-calibrated with the ^{40}K in the PMTs, by considering the Compton electrons crossing the detector.

An accurate time calibration is necessary for t-o-f discrimination. The relative timing offsets between scintillators were determined with a ^{60}Co source placed in the center of the detector.

Leading edge discriminators were used, so the timing signal is energy dependent. To determine this dependence, a nitrogen pulsed UV laser (VSL337 LSI) whose pulses have a duration of 3 ns and whose output amplitude is adjusted by a set of calibrated attenuators is simultaneously sent to each scintillator through plastic optical fibers.

The intensity of the laser light is monitored by a calibration reference photodiode (S2743N Hamamatsu) that receives both the laser signal and alpha particles emitted by an ^{241}Am source (Fig. 8). This laser device performs the time calibration with a fast XP2020 PMT that receives the laser signal and provides the timing reference. During a laser calibration run the XP2020 PMT provides a programmable delayed common STOP to all the scintillator modules.

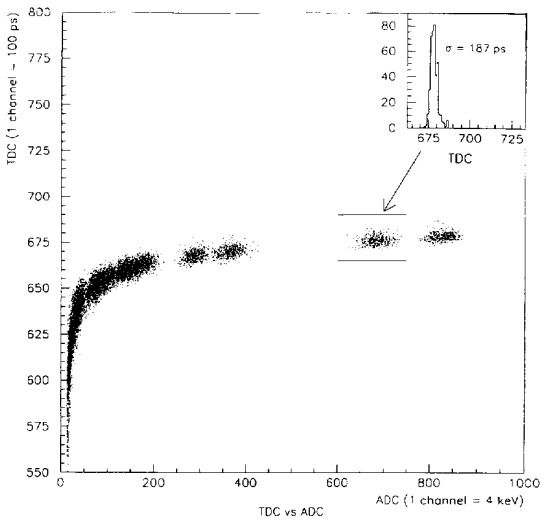

Fig. 9. Response of the TDC and ADC of a counter to different intensities of the calibration laser.

The response of the ADC and the TDC to the laser pulses for each channel is recorded for different amplitudes of the laser signal (Fig. 9). The energy dependence of the timing signal is then parametrized with

$$F(\mathrm{adc}) = p_1 - \frac{p_2}{\mathrm{adc}} - \frac{p_3}{\mathrm{adc}}\exp\left(-\frac{p_4}{\mathrm{adc}}\right) \quad (2)$$

where adc is the charge amplitude of the signal (in channels) and p_i are fitted parameters for each scintillator. This relation is obtained after considering the expression of the time dependence of the voltage pulse expected at the anode which in turn depends on the decay constant of the scintillator, the circuit time constant, and the total charge.

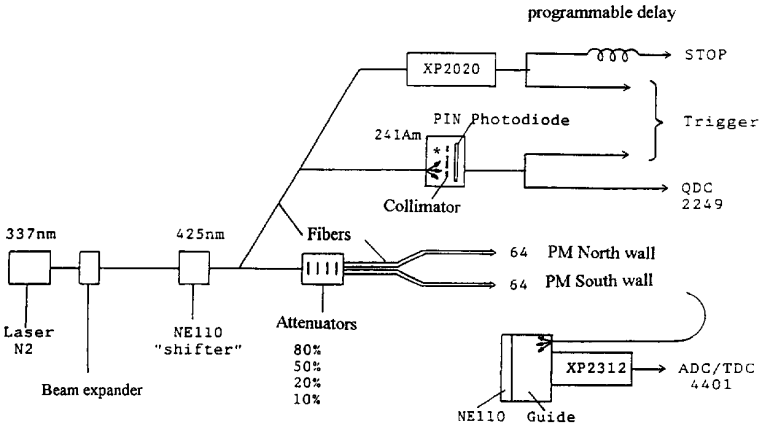

Fig. 8. Diagram of the calibration laser and optical fibers device.

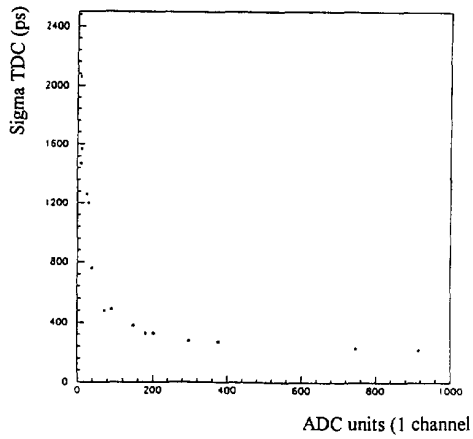

Fig. 10. Time resolution versus ADC channels for a single scintillator module.

The recorded time which will be used for t-o-f calculation is given by:

$$\mathrm{tdc}_{\mathrm{corrected}} = \mathrm{tdc} - F(\mathrm{adc}) \qquad (3)$$

where tdc is the recorded time in channels.

As shown in Fig. 10, the timing resolution for a typical counter is $\sigma = 250$ ps at 1 MeV but reaches 450 ps below 200 keV. Consequently, to maintain good time resolution, all the experimental data were analyzed with an energy cut at 200 keV.

In an experiment which requires long and continuous running time with a large number of PMTs, performing frequent tests on the system's stability is essential. The laser and optical fibers calibration device enables daily checking of the energy and time calibrations. The daily energy and time variations (Fig. 11) are then corrected off-line by software. The long term stability is better than 4% in energy and 200 ps in time.

4. Background studies

4.1. General considerations

In a very low-counting rate experiment such as this double beta decay experiment, it is essential to understand all components of the background, in order to reduce it as much as possible. Elementary steps were taken to reduce the background intensity. The cosmic-ray activity is reduced by placing the experiment in an underground laboratory. Next the detector must be shielded against radioactivity of the rock and surrounding materials. Finally the detector's components must be carefully selected for their low levels of radioactivity.

In the NEMO 2 experiment, the source is mounted on a removable frame in the middle of the detector. This makes it easy to put different sources under study. Initially a natural molybdenum foil (50 μm), from a commercial source, containing rather high levels of radioactive contamination (≈ 1 Bq in ^{214}Bi), and a purified natural molybdenum foil (50 μm) were inserted into the detector in order to study the background components produced by contamination in the foil. Then an OFHC copper foil known for its ultra low radioactivity was used to measure the background components induced by all other parts of the detector. The thickness of this foil (70 μm) was chosen to provide roughly the same stopping power as the natural molybdenum foil for low energy electrons.

In this section, the "external background" is defined as events created by the radioactivity located in the components of the detector, other than the central foil, and the

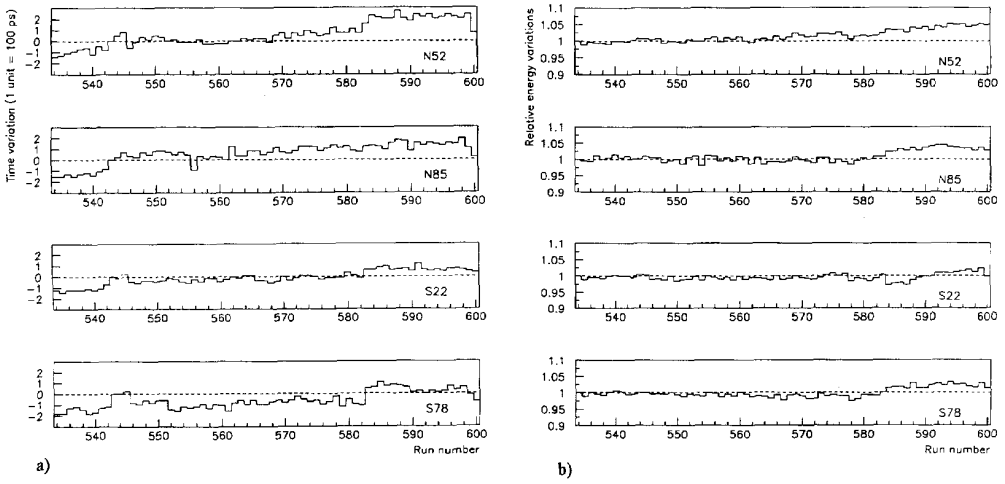

Fig. 11. a) Observed variation of the time signal for two scintillators of each array. b) Observed variation of the relative energy gain for scintillators. The variations are used as corrections in off-line analysis (1 run per day).

"internal background" as events initiated by radioactive contaminants contained in the foil. In order to understand the importance of backgrounds and the signal-to-noise ratio, we have considered a signal emitted from a virtual 1 m^2 by 50 μm thick 100% enriched "reference ^{100}Mo foil" placed in NEMO 2 with $T_{1/2}(\beta\beta 2\nu) = 10^{19}$ years [10] and a 2% detection efficiency. The expected event rate is approximately 0.5 ($\beta\beta 2\nu$) events/h. This calculation will be referred to for comparisons in the following discussion. After discussing the external and internal background components, the detector's sensitivity to radon, the effect of the residual cosmic-rays (muons) and neutrons will be presented.

4.2. The "external" radioactivity background

An extensive program of material selection and control, using γ-ray spectrometry with very low background HPGe detectors, was initiated several years ago in the Fréjus underground laboratory [11]. These spectroscopic measurements ensure that the materials composing the detector have very low level of natural, artificial (^{137}Cs and ^{60}Co) and cosmogenic radioactive contamination. The standard level of sensitivity of contamination detection with a Ge detector is around 0.02 Bq/kg and the ultimate level of sensitivity using 1 kg samples and measuring for two weeks yields levels of 1 mBq/kg. This selection process in NEMO 2 showed that the external background for energies lower than 3 MeV is dominated by the radioactivity of the PMTs.

At the beginning of the experiment, only PMTs made from common glass were available. This glass was known to have high levels of ^{40}K, ^{214}Bi and ^{208}Tl [10] which generate a relatively intensive γ-ray flux. These photons interact with the plastic scintillator via Compton interactions. The Compton electron can then cross the two drift chambers and deposit energy in a scintillator on the opposite wall. This type of event mimics double beta decay events, and is rejected by t-o-f considerations.

The rejection criterion is based on the comparison of the measured t-o-f (ΔT_m) with calculated ones, assuming first that a single electron crosses the detector (ΔT_e) and then that two electrons are emitted from the central source (ΔT_i). The calculation of a theoretical t-o-f takes into account the energy dependent velocity of the electron(s). In the first hypothesis where a single electron crosses the detector, the electron's energy used for (ΔT_e) calculation is given by the arrival scintillator's ADC. In the second hypothesis where two electrons are emitted from the central foil, the energies used for (ΔT_i) calculation are given by the two triggered scintillator ADCs. In both cases the ADC values are corrected for the energy losses of the electron(s) along their path. Fig. 12 represents $|\Delta T_m - \Delta T_i|$ versus $|\Delta T_m| - \Delta T_e$ for two-track events recorded on molybdenum foils. The plot presents two well-separated bumps. The events for which two electrons are emitted

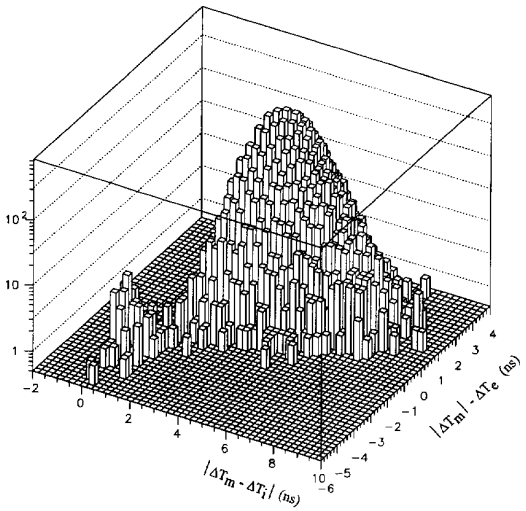

Fig. 12. $|\Delta T_m - \Delta T_i|$ versus $|\Delta T_m| - \Delta T$ distribution for non-filtered two-track events recorded on purified and enriched molybdenum foils for 240 h of data collection (in ns). The through going electrons correspond to the $|\Delta T_m| - \Delta T_e$ distribution around 0 ns, whereas the electrons emitted from the central source correspond to the $|\Delta T_m - \Delta T_i|$ distribution around 0 ns (the variables ΔT_m, ΔT_e and ΔT_i are defined in the text).

from the central foil are centered around $|\Delta T_m - \Delta T_i| \approx 0$ ns. The events associated with electrons crossing the detector have $|\Delta T_m| - \Delta T_e \approx 0$ ns. The rejection factor is greater than 5×10^4.

The photons emitted by the PMTs can also interact on the central foil. In this case they can produce either two successive Compton electrons, or a Compton electron followed by Möller scattering, or pair production. When photons released in these interactions are not detected, the resulting events are considered to be genuine electron-electron events. This type of event whose t-o-f difference is centered about at 0 ns, mimic double beta decay events.

To measure this residual background, two-track events recorded with the copper foil were analyzed. The resulting energy spectrum is plotted in Fig. 13 for 2240 hours of data collection. For these events it was required that no CsI was fired (γ veto) and the energy deposit in each scintillator was greater than 200 keV. In this spectrum one recognizes the main contribution of the ^{40}K contained in the glass of the PMTs. Note that no event occurred with an

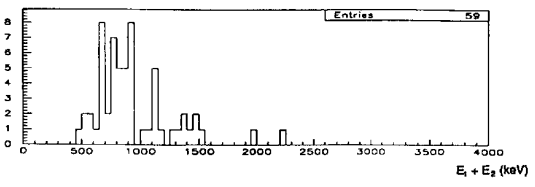

Fig. 13. Electron summed energy spectrum of two-track events recorded using the copper foil for a 2240 h exposure.

energy greater than 2.2 MeV although the most energetic γ-ray of natural radioactivity, which is produced by ^{208}Tl, is 2.614 MeV. This shows that the external events should not be a troublesome background source for the ($\beta\beta0\nu$) measurements (^{100}Mo, $Q_{\beta\beta} = 3.03$ MeV). On the other hand the counting rate and the shape of this background spectrum are limitations in a ($\beta\beta2\nu$) measurement. The extrapolation of the external two-track event rate measured using the copper foil, yields 0.1 external two-track events/h on the reference molybdenum foil previously defined. Therefore to ensure the measurement of ($\beta\beta2\nu$) half-life greater than 10^{19} years, the photomultipliers have recently been replaced with less radioactive ones, which are now commercially available.

4.3. The "internal" radioactivity background

The radioactivity contained in the central foil produces beta emissions followed by either conversion electrons or Möller scattering. These decays also produce two-track events with t-o-f differences almost ≈ 0 ns not unlike double beta decay events. From γ-ray spectroscopy it is known that the main radioactive contaminants in the central foil are uranium and thorium progenies from the natural radioactivity chains. For ($\beta\beta0\nu$) in ^{100}Mo, the ^{214}Bi ($Q_\beta = 3.27$ MeV) and the ^{208}Tl ($Q_\beta = 4.99$ MeV) decays are the only background radioactive isotopes which must be considered. In ($\beta\beta2\nu$) three other isotopes with $Q_\beta \approx 2$ MeV must be taken into account, ^{234m}Pa, ^{228}Ac, and ^{212}Bi decays. According to Monte-Carlo calculations, if a molybdenum foil, with the same dimensions as our reference foil, contains 1 Bq/kg of ^{214}Bi or ^{208}Tl, an internal background rate of 2 electron–electron events/h is expected from each of these nuclei. Consequently a careful purification process of the central foil is necessary.

The experimental two-electron energy spectrum of internal background events in the commercial molybdenum foil, is compared to a simulated one in Fig. 14. The simulation is performed with GEANT [3] (version 3.15) which correctly treats the low energy electrons. Standard isotope decay schemes were applied [13] and unknown conversion coefficients were calculated from theoretical tables [14]. The levels of activities of the various contaminants were provided by the γ-ray spectroscopy.

Several other event topologies may be investigated with NEMO 2. Even if two-track events are of primary interest for double beta decay investigations other channels, such as (e), (e, γ), (e, γ, γ) and (e, γ, α), can be studied since they also contribute to the understanding of the background.

[3] GEANT user guide, CERN, DD/EE/83I

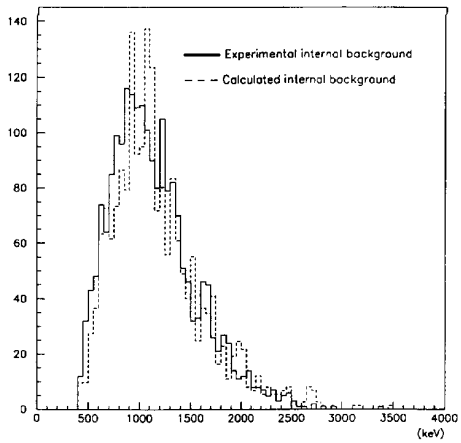

Fig. 14. Experimental and simulated energy spectra for two-track events using the commercial molybdenum foil for 2200 h of data collection.

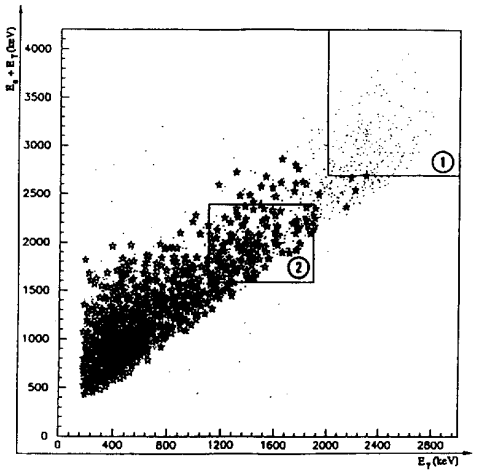

Fig. 15. Sum of gamma and electron energies versus gamma energy for simulated (e, γ) events produced by ^{214}Bi (stars) and ^{208}Tl (points). The energy region (①) with $E_\gamma + E_e > 2.7$ MeV and $E_\gamma > 2$ MeV contains only events created by the ^{208}Tl whereas the energy region (②) $1.6 < E_\gamma + E_e < 2.4$ MeV and $1.1 < E_\gamma < 1.9$ MeV contains events from ^{214}Bi and ^{208}Tl.

Table 2
^{214}Bi and ^{208}Tl contamination measured with a HPGe detector and the NEMO 2 detector for commercial and purified natural molybdenum foils

Detector	Commerical Mo (Bq/kg)		Purified Mo (Bq/kg)	
	^{214}Bi	^{208}Tl	^{214}Bi	^{208}Tl
Ge	1.5 ± 0.2	0.12 ± 0.03	< 0.02	< 0.007
NEMO 2	1.1 ± 0.1	0.105 ± 0.012	< 0.02	< 0.002

4.3.1. The (e, γ) channel

The analysis of the NEMO 2 experimental data to measure ^{214}Bi and ^{208}Tl contamination is possible by considering the (e, γ) channel. This type of event corresponds to a beta decay of a nucleus within the central foil, accompanied by gamma ray emission. The photon is identified as a trackless scintillator event with an energy deposit greater than 200 keV, possibly accompanied by a signal from the CsI. Timing conditions select internal events. However, in spite of these t-o-f cuts, (e, γ) events initiated on the central foil by Compton interactions of external photons are not rejected. Fig. 15 shows a plot of the sum of the gamma and electron energies versus the gamma energy obtained with Monte-Carlo simulations. From the experimental data, using the displayed cuts and the corresponding computed detection efficiencies, a deduced ^{214}Bi and ^{208}Tl contamination level is made after subtraction of the external background components measured using the high purity copper foil.

Following this procedure, the activities (or their limits) of two molybdenum foils with different levels of radioactivity were measured with NEMO 2. The results are in good agreement with the γ-ray spectroscopy measurements, as shown in Table 2. The sensitivity is again limited by the intensity of the external background. The sensivity of the ^{214}Bi activity measurement is slightly improved by approximately a factor of 2 for the "back-to-back events", in which the electron and γ-rays are detected in opposite arrays, since the external background due to photons coming from the PMTs, after t-o-f cuts, is mainly composed of "same side events".

4.3.2. The (e, γ, γ) channel

Another way to measure the ^{214}Bi and ^{208}Tl activities is to investigate the (e, γ, γ) channel. A study of this channel enables a strong rejection of the external background. With the usual t-o-f cut it is enough to require the photons be "back to back". This analysis has led to the following limits for the purified natural molybdenum source: < 0.04 Bq/kg for the ^{214}Bi and < 0.02 Bq/kg for the ^{208}Tl activities on the purified natural molybdenum foil. The low detection efficiency of the photons explains that the resulting limits are less stringent than those contained in Table 2.

4.3.3. The (e, γ, α) channel

Delayed alpha particles are expected in the ^{214}Bi beta decay when the daughter ^{214}Po, emits an alpha particle of 8 MeV with a half-life of 164 μs. Because of their great ionizing power, the alpha particles have a maximum range of 30 cm in the helium gas. Thus short tracks, composed of at least three delayed Geiger cell planes, characterize these alpha particles. The experimental delay time distribution for (e, γ, α) events recorded with a vertex on the commercial natural molybdenum foil is given in Fig. 16. The exponential fit to the 400 h run leads to a half-life of

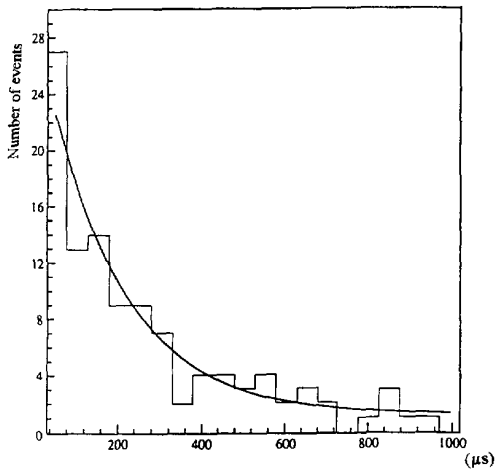

Fig. 16. Alpha radioactive decay, from (e, γ, α) events during 400 h of data collection on the commercial natural molybdenum foil.

(165 ± 44) μs which is compatible with the 164 μs expected value. Taking into account the detection efficiency 0.52% for (e, γ) events and the 5% probability that the alpha particle escapes the foil, the ^{214}Bi activity of the commerical molybdenum foil was 1.3 ± 0.4 Bq/kg. This result is in agreement with the previous measurements (Table 2). The activity measurements are not significantly affected by the radon rate in the laboratory, as shown in section 4.4, and the possible activity in ^{214}Bi generated by the accumulation of radon on the central foil is two orders of magnitude smaller.

4.3.4. The (e) channel

A beta particle emitted from the central source can induce, by Möller scattering, an electron–electron event mimicking double beta decay. In the NEMO 2 detector an estimation of the total activity of the single beta emitters which are not detectable by γ-ray spectroscopy, such as ^{90}Y ($Q_\beta = 2.3$ MeV) from ^{90}Sr or ^{234m}Pa ($Q_\beta = 2.2$ MeV) isotopes contained in the source, can be made. Such an estimation was obtained through the analysis of one-track data recorded on the purified natural molybdenum foil. Only electrons with an energy above 1.2 MeV were selected, in order to eliminate the external events produced by the ^{40}K in the PMTs. Using the computed detection efficiencies of single electron events, a 0.07 Bq/kg limit on the beta emitter activity was measured on the natural molybdenum foil. Considering the above mentioned "reference molybdenum foil" (see Section 4.1), such a limit leads to less than 0.03 Möller induced two-track events/h. Of course the analysis is only relevant for sources for which the ^{214}Bi and ^{208}Tl activities are very weak and do not dominate this energy region.

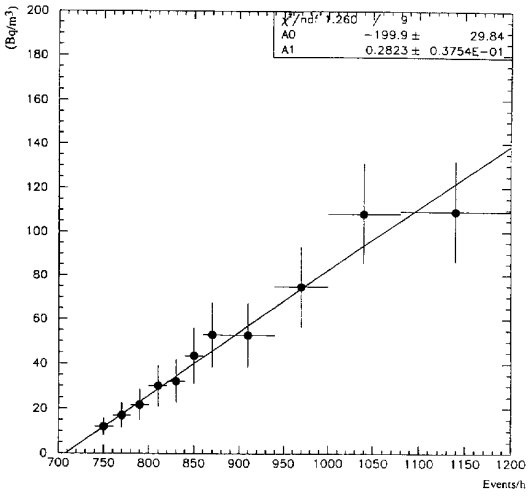

Fig. 17. Radon rate (in Bq/m^3) as measured in the laboratory versus the experimental trigger rate.

4.4. The effects of radon

The radon gas contained in the laboratory, with its ^{214}Bi daughter, constitutes another background source for the experiment. The presence of radon is due to the out-gassing of the surrounding rock. Continuous monitoring of the radon level inside the laboratory shows variations from 20 Bq/m^3, which is the normal rate, to some momentary peaks at 150 Bq/m^3 when the laboratory ventilation is restricted.

Fig. 17 demonstrates a linear correlation between the trigger rate of the experiment and the mean radon level measured inside the laboratory. The experimental trigger rate is largely dominated by Compton electrons created in the scintillators and crossing the chamber. Therefore the recorded increases in the trigger rate are due to an obvious increase of the external γ-flux induced by the radon daughter ^{214}Bi.

Table 3
Counting rates for (e, γ) and (e, e) events for runs of low and high radon levels recorded using a purified 50 μm Mo foil

Event channel	Radon level < 30 Bq/m^3 $\Delta t = 2816$ h (events/hour)	Radon level > 100 Bq/m^3 $\Delta t = 510$ h (events/hour)
(e, γ)	0.76 ± 0.03	1.19 ± 0.03
(e, e)	0.067 ± 0.005	0.106 ± 0.015

In order to quantify the effect of radon on the (e, e) and (e, γ) channels, an analysis was performed on the experimental data recorded using the purified natural molybdenum foil during run times with different radon levels. The results are presented in Table 3. These event rates prove that the radon significantly affects both the (e, e) and (e, γ) channels by an augmentation of the external γ-ray flux. The possibility of radon daughters being deposited on the central foil was studied analyzing (e, γ, α) events recorded on the purified molybdenum foil. The (e, γ, α) events whose reconstructed vertex was on the central foil (Fig. 18a) were differentiated from those whose vertex was in the tracking volume (Fig. 18b). The corresponding counting rates for low and high radon levels are given in Table 4. In spite of the low counting rates it is obvious that there is radon contamination in the helium gas and that radon daughters are deposited on the central foil. This problem is a result of radon diffusion through the external mylar windows. Because of the radon deposited on the central foil, the experiment's ability to measure the internal ^{214}Bi contamination is limited to 0.01 Bq/kg through the (e, γ) channel. To prevent the radon contamination a technique which is under development employs a radon resident

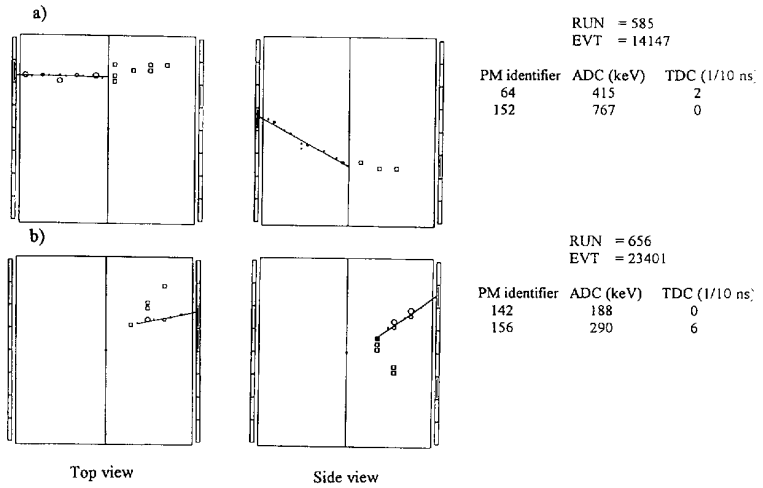

Fig. 18. (e, γ, α) events whose reconstructed vertex is a) on the central foil, and b) in the drift chamber. The Geiger cells triggered by these alpha particles have approximately 4 μs delays, and are represented by small squares.

Table 4
Counting rates for (e, γ, α) events recorded on a purified molybdenum foil and in the tracking volume for runs of low and high radon level

(e, γ, α) events	Low radon level $\Delta t = 5287$ h (events/1000 h)	High radon level $\Delta t = 535$ h (events/1000 h)
Foil	8 ± 1	32 ± 6
Tracking volume	15 ± 2	28 ± 7

shield that also traps the radon in the air which circulates inside the shield.

4.5. Cosmic rays and neutrons

In this experiment cosmic rays and neutrons are the main possible origins of high energy two-track events (> 3 MeV). These events are potentially the most troublesome external background component in the search for the $(\beta\beta 0\nu)$ decay process. The cosmic muon rate in the L.S.M. is 4.2 m^{-2} d^{-1} [15]. All the muons crossing the detector are easily identifiable by their 3 ns t-o-f. These muons are minimum ionizing particles and leave the same energy (≈ 3.5 MeV) in each scintillator while saturating the ADC of the associated CsI.

The natural radioactivity generates a neutron flux when neutrons are released during spontaneous fissions and (α, n) reactions. The capture of thermalized neutrons by copper ($\sigma = 4.4$ b) and iron ($\sigma = 2.2$ b) generates γ-rays with energies up to 8 MeV. These energetic γ-rays induce incoming Compton electrons and electron–electron events on the central foil chiefly through pair production and second order processes.

In order to study the effect of neutrons on the NEMO 2 detector, an Am–Be neutron source (2×10^4 decays/s) was placed outside of the shield at a distance of 2.5 m from the centre of the detector for 3.6 h. Fig. 19a shows the resulting spectrum of the electrons crossing the detec-

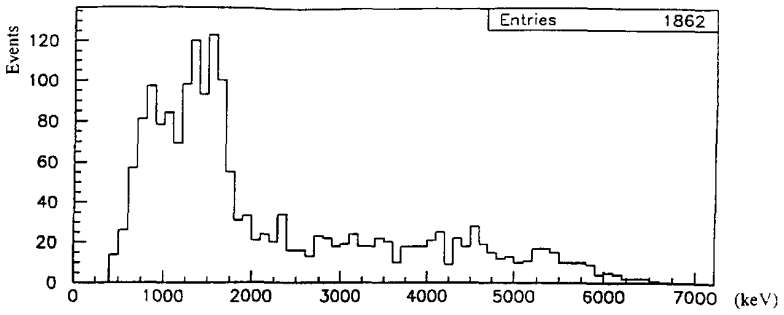

a)

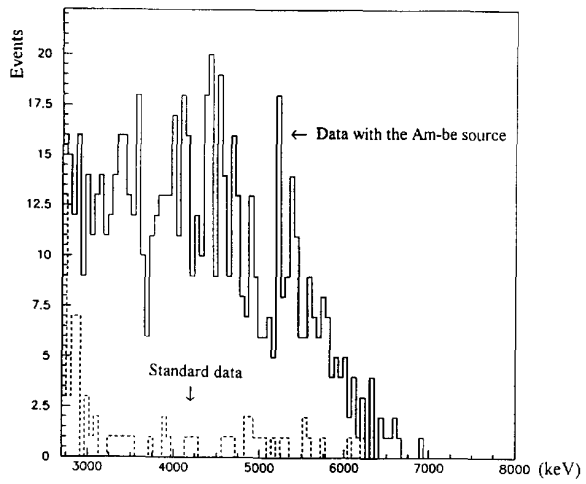

b)

Fig. 19. a) Energy spectrum of through going electron events recorded during an exposure of NEMO 2 to an Am–Be source for 3.6 h. b) Neutron induced events for E > 2.7 MeV. The solid line is the high energy region of (a). The dashed line is the observed spectrum corresponding to 6100 h of normal operation with muon events removed.

tor with no t-o-f cut. Fig. 19b shows the high energy part of this spectrum which is compared to the spectrum obtained without the neutron source on the purified natural molybdenum foil in 6100 h exposure. Assuming the energy spectrum of the photons generated by the neutron source behaves like the spectrum due to the ambient neutron flux, the short neutron run corresponds to 10 years of standard data collection.

Applying the usual t-o-f conditions to the neutron source spectrum, in terms of rates, 0.5 electron–electron events/(yr MeV) neutron induced events are expected below 3 MeV. This neutron background is negligble for $(\beta\beta 2\nu)$ investigations. Whereas the expected residual rate of about 0.1 electron–electron events/(yr MeV) neutron induced events in the 3 MeV region, is troublesome for $(\beta\beta 0\nu)$ investigations. Since this background is mainly composed of (e^+, e^-) events created in the central foil, a magnetic field would provide a signature to identify these events.

5. Conclusion

The NEMO 2 detector is the second prototype of a long-term project to study double beta decay. This experiment has been running successfully since August 1991. The Geiger cell drift chambers track the electrons emitted from a source foil while the through going electrons are rejected by t-o-f criteria. Plastic scintillator walls provide the energy and t-o-f information. As every low-counting rate experiment, it is located in an underground laboratory to escape cosmic rays, and all the materials composing the detector have been selected for their low levels of radioactivity using γ-ray spectrometry.

The ability of NEMO 2 to investigate various types of events with different central sources enabled a detailed analysis of the various sources of background. Thus, it is known that the external background is mainly due to the radioactivity of the PMTs, as concluded from measurements with a high purity copper foil. The ^{214}Bi and ^{208}Tl contamination in the source foils was measured by γ-ray spectroscopy, and found to be consistent with the NEMO 2 data analysis of the (e, γ), (e, γ, γ) and (e, γ, α) channels.

As expected the (e, γ) and the (e, e) rates are influenced by the radon level inside the laboratory. To reduce this effect the volume of air within the shield should be minimized. Additionally a radon tight shield with a facility to trap radon within the shield should be instrumented. Such a device is being developed. For cosmic rays the resulting (e, e) events are unambiguously rejected by t-o-f. The effect of the residual neutron flux is negligible for $(\beta\beta 2\nu)$ measurements whereas it can generate a significant background for $(\beta\beta 0\nu)$.

Although this detector was primarily devoted to background studies, it was able to measure the half-life $(\beta\beta 2\nu)$ in ^{100}Mo with a good statistics [8]. Currently a second set of $(\beta\beta 2\nu)$ measurements with new low radioactive PMTs is in progress. Subsequently a clear understanding of the background components will allow the successful construction of a larger detector, NEMO 3 [16], which will house a 20 m^2 central foil of 10 kg of enriched material.

References

[1] H.V. Klapdor and B. Povh, Proc. Int. Workshop, Heidelberg, Germany, 1987 (Springer);
F. Boehm and P. Vogel, Physics of Massive Neutrinos, 2nd ed. (Cambridge University Press, 1992).
[2] F.T. Avignone III and R.L. Brodzinski, Prog. Part. Nucl. Phys. 21 (1988) 99.
[3] M.K. Moe, UCI-NEUTRINO 93–1 (Feb. 1993).
[4] M.K. Moe and P. Vogel, UCI-NEUTRINO 94–5 (Feb. 1994).
[5] D. Dassié et al., Nucl. Instr. and Meth. A 309 (3) (1991) 465.
[6] R. Arnold et al., XV Int. Conf. on Neutrino Physics and Astrophysics (NEUTRINO 90), Granada, Spain, 1992.
[7] R. Arnold et al., Int. Europhys. Conf. on High Energy Physics, Marseille, France, 1993.
[8] R. Arnold et al., Two-neutrino double beta decay measurement of ^{100}Mo (To be published in Phys. Rev.).
[9] R. Frühwirth et al., Nucl. Instr. and Meth. A 262 (1987) 444.
[10] H. Ejiri et al., Phys. Lett. B 258 (1991) 17;
R. Elliot et al., J. Phys. G. Nucl. Part. Phys. 17 (1991) S145.
[11] J. Busto et al., Second Int. Workshop on Theoretical and Phenomenological Aspects of Underground Physics, Toledo, Spain, 1991; Nucl. Phys. B. (Proc. Suppl) 28 A (1992) 425.
[12] P. Jagam and J.J. Simpson, Nucl. Instr. and Meth. A 324 (1993) 389.
[13] C.M. Lederer and V.S. Shirley (eds.), Tables of Isotopes (Wiley-Interscience, 1978).
[14] K. Way (ed.), Internal Conversion Coefficients, Atomic and Nuclear Data Reprints, vol. 1 (1973).
[15] Ch. Berger et al., Nucl. Instr. and Meth. A 262 (1987) 463.
[16] R. Arnold et al., Nucl. Phys. B (Proc. suppl.) 35 (1994) 369.